Rectification of the Madden–Julian Oscillation into the ENSO Cycle

WILLIAM S. KESSLER

NOAA/Pacific Marine Environmental Laboratory, Seattle, Washington

RICHARD KLEEMAN*

Bureau of Meteorology Research Center, Melbourne, Australia

(Manuscript received 1 February 1999, in final form 16 August 1999)

ABSTRACT

An ocean general circulation model, forced with idealized, purely oscillating wind stresses over the western equatorial Pacific similar to those observed during the Madden–Julian oscillation (MJO), developed rectified low-frequency anomalies in SST and zonal currents, compared to a run in which the forcing was climatological. The rectification in SST resulted from increased evaporation under stronger than normal winds of either sign, from correlated intraseasonal oscillations in both vertical temperature gradient and upwelling speed forced by the winds, and from zonal advection due to nonlinearly generated equatorial currents. The net rectified signature produced by the MJO-like wind stresses was SST cooling (about 0.4°C) in the west Pacific, and warming (about 0.1°C) in the central Pacific, tending to flatten the background zonal SST gradient. It is hypothesized that, in a coupled system, such a pattern of SST anomalies would spawn additional westerly wind anomalies as a result of SST-induced changes in the low-level zonal pressure gradient. This was tested in an intermediate coupled model initialized to 1 January 1997, preceding the 1997–98 El Niño. On its own, the model hindcast a relatively weak warm event, but when the effect of the rectified SST pattern was imposed, a coupled response produced the hypothesized additional westerlies and the hindcast El Niño became about 50% stronger (measured by east Pacific SST anomalies), suggesting that the MJO can interact constructively with the ENSO cycle. This implies that developing the capacity to predict, if not individual MJO events, then the conditions that affect their amplitude, may enhance predictability of the strength of oncoming El Niños.

1. Introduction

The regular occurrence of enhanced intraseasonal variability over the western equatorial Pacific during the onset stage of El Niño has fostered a wide-ranging debate over the possible role of the Madden–Julian oscillation (MJO; Madden and Julian 1972, 1994) in the El Niño–Southern Oscillation (ENSO) cycle. There are at least two viewpoints currently existing on this subject. First, since coupled models without the MJO are capable of skillful ENSO forecasts, one school of thought holds that there is little influence (e.g., Zebiak 1989). This viewpoint notes that some level of MJO activity occurs over the west Pacific nearly every year, El Niño or not, and therefore argues that the spatial–temporal characteristics of the MJO are not of fundamental importance. On the other hand, since the surface wind and flux pattern of the MJO (giving rise to zonal gradients along the equator) suggests an efficient projection onto low-frequency ENSO-like modes, another school argues that the MJO can act as a disruptive or stochastic influence on an otherwise regular ENSO cycle and thereby contribute to the observed irregularity (Moore and Kleeman 1998).

The present paper examines physical processes that might produce coupling between the MJO and the ENSO cycle. Many observers have pointed out that the propagation of oceanic Kelvin waves leads to prominent MJO signatures in thermocline depth in the east, where SST is highly sensitive to the vertical temperature gradient (Kessler and McPhaden 1995; McPhaden 1999). However, while the propagating thermocline signals can be impressively large, a nonlinear process would be necessary to couple intraseasonal and interannual frequencies, but this has been difficult to demonstrate (see Kessler et al. 1995 for one example). The purpose of the present study is to investigate nonlinear mechanisms by which the oscillating winds of the MJO could have a rectified effect on the ocean–atmosphere system.

The longest time series showing the spatial–temporal

* Current affiliation: Courant Institute for Mathematical Sciences, New York University, New York, New York.

Corresponding author address: William S. Kessler, NOAA/PMEL/OC, 7600 Sand Point Way NE, Seattle, WA 98115.
E-mail: kessler@pmel.noaa.gov

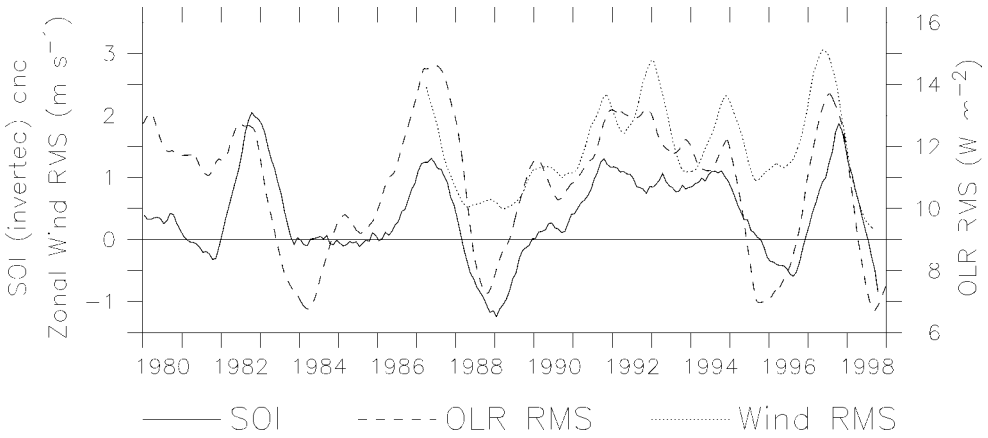

FIG. 1. Time series of the SOI (line), OLR intraseasonal rms, averaged in the region 2°S–2°N, 155°–175°E (dash, W m^{-2}), and zonal wind intraseasonal rms at the TAO mooring at 0°, 165°E (dotted line, m s^{-1}). The SOI is inverted (so El Niño events are positive on the plot).

evolution of intraseasonal variability is the regular satellite measurements of outgoing longwave radiation (OLR) that have been made continuously since 1979. OLR is a measure of tropical deep convection, and numerous studies have used coherent aspects of its intraseasonal variability to indicate the MJO (Knutson and Weickmann 1987; Rui and Wang 1990; Hendon and Salby 1994; Zhang and Hendon 1997; Shinoda et al. 1998; Hendon et al. 1999). We constructed an index of intraseasonal activity over the west Pacific warm pool by bandpassing OLR (approximately between 25- and 120-day periods), averaging within 2°S–2°N, 155°–175°E, then squaring these values and plotting the square root of the 1-yr running mean of the resulting time series (Fig. 1). A similarly constructed index was made from the only long time series of in situ winds in the western equatorial Pacific, at the Tropical Atmosphere–Ocean (TAO) mooring at 0°, 165°E (see section 2c), and is also plotted in Fig. 1. Comparing these indexes with the Southern Oscillation Index (SOI) shows that warm pool intraseasonal rms roughly doubled during each of the El Niño events of the past 18 years; the lag correlation between OLR and SOI is 0.74, with OLR leading by about 70 days (the correlation is significant above the 95% level; see appendix A). The zonal wind index is also highly correlated with the SOI ($r = 0.80$), showing the clear association of intraseasonal zonal winds with the onset of recent El Niño events. The high correlation among the three quantities is due to the eastward spread of intraseasonal activity over the west Pacific early in El Niño events, reflecting the fact that as warm SST expands eastward during the growth stage of El Niño, convection tends to follow (Fink and Speth 1997). However, we note that only perhaps half the intraseasonal variance is associated with the eastward-propagating, spatially coherent global mode (often measured by 200-mb zonal winds) that defines the MJO (Slingo et al. 1999; Hendon et al. 1999). In contrast to the present warm pool intraseasonal index, the overall level of global MJO activity is not well correlated with the ENSO cycle. Although the low zonal-wavenumber MJO does not alter its overall character due to the ENSO cycle, convection associated with individual MJO events occurs over warm SST and therefore can extend farther east with the onset of El Niño, without necessarily producing a large change in the global MJO mode. In any case, Fig. 1 shows that the early stages of El Niño events are associated with a significant increase in intraseasonal activity over the warm pool. Of course, the high correlation seen in Fig. 1 does not imply causality, and it remains possible that the enhanced intraseasonal variance is an incidental symptom of advancing El Niño conditions but not an essential feature of it. Nevertheless, the regular association between these two signals at different frequencies raises the question of whether nonlinear interaction might occur. In the rest of this paper we evaluate potential mechanisms through which the correlations seen in Fig. 1 might in fact represent an active and constructive element of the ENSO cycle.

The focus here is on rectified nonlinear changes in the ocean in response to oscillating winds, and how this response could feed back to modify the lower-frequency coupled system. From another point of view, there is a rich literature on air–sea interactions associated with the atmospheric thermodynamics of the MJO (Emanuel 1987; Neelin et al. 1987; Lau et al. 1989; Webster 1994; Hendon and Glick 1997; Jones et al. 1998), and a useful schematic overview of several theories is given in Flatau et al. (1997).

In the present research, two separate models were used in series to understand the effect on the coupled system of intraseasonal winds. First, an ocean general circulation model (OGCM) was used to investigate the (nonlinear) effects on the ocean of imposed intraseasonal zonal winds, then a much simpler intermediate

coupled model was used to evaluate the effects of the resulting SST pattern on the coupled system during the onset of El Niño. While this procedure is somewhat indirect and risks missing coupled feedbacks that might occur on the intraseasonal timescale itself, it makes diagnosis of the oceanic physical mechanisms more straightforward than would be possible in a coupled GCM context. A posteriori, the subtlety of some aspects of these mechanisms bears out the utility of isolating the two systems, at least for the initial examination of these phenomena as conducted here.

Section 2 of this paper discusses the two models used to study these phenomena, and how the idealized forcing fields were imposed. Section 3 describes the rectified signals in the ocean due to imposed intraseasonal winds, and diagnoses the mechanisms responsible for the rectification. Section 4 shows results from the coupled model experiments, and section 5 discusses the implications with regard to the ENSO cycle. Note that here we use the term ''low frequency'' to refer to periods of more than a few months, unlike much of the atmospheric literature in which intraseasonal periods themselves are considered low frequency.

2. Model formulations and data processing

a. Ocean general circulation model

The tropical upper ocean GCM used in this study consists of two physical components: a sigma-layer, tropical primitive equation general circulation model developed by Gent and Cane (1989), with the ''hybrid'' mixed-layer formulation developed by Chen et al. (1994a,b) as its surface boundary layer. The entire model domain is the upper active layer (roughly 400-m thick) of a reduced-gravity ocean, assumed to overlie an infinitely deep, motionless abyss. There is thus no bottom topography. The model consists of eight sigma levels within the active upper layer, and the surface mixed layer. External forcing of the model is through specified wind stresses and clouds only, according to the heat flux formulation of Seager et al. (1988).

The hybrid mixing scheme of Chen et al. (1994b) defines a turbulent boundary layer that exchanges momentum and heat with the atmosphere at its surface and with the thermocline by entrainment at its base. The three major physical processes of upper-ocean turbulent mixing are explicitly simulated. Mixed-layer entrainment and detrainment are related to wind stirring and surface buoyancy (heat) flux using a bulk mixed-layer (Kraus and Turner 1967) model, shear flow instability is accounted for by partial mixing controlled by the gradient Richardson number, and an instantaneous adjustment parameterizes free convection (Price et al. 1986). In essence this combines the most physically realistic features of a bulk mixed-layer model with those of an instability mixing model (Chen et al. 1994b).

The model domain is the equatorial Pacific with solid walls at 30°S and 30°N and no opening through the Indonesian Archipelago, but otherwise realistic east and west coasts. A stretched grid is used in which the zonal spacing is smallest at the east and west edges (Δx about 50 km) and largest in midbasin (Δx about 120 km) while the meridional spacing is smallest within 10°N and 10°S (Δy about 40 km) and largest at the poleward edges (Δy increases to about 220 km). The time step is 1 h. The model is initialized with the Levitus (1982) mean temperatures (and zero currents). Relaxation to the Levitus climatological annual cycle temperatures becomes progressively stronger poleward of $\pm 20°$ latitude to suppress coastal Kelvin waves that would otherwise contaminate the solution given these unrealistic poleward boundaries. In the present formulation the equation of state is a linear function of temperature, with no effect of salinity, although variations of salinity are likely to be an important contribution to density changes in the tropical Pacific (Murtugudde and Busalacchi 1998; Ji et al. 2000; Kessler 1999).

Average annual cycle forcing fields were used to spin up the model. The wind stress climatology was made from the Florida State University wind product (Stricherz et al. 1992) for the period 1961–91, with a constant drag coefficient $c_D = 1.4 \times 10^{-3}$. Clouds were based on the 1983–94 International Satellite Cloud Climatology Project C2 product (Rossow and Schiffler 1991), with solar radiation derived from solar harmonics and bulk formulas used for latent, longwave, and sensible heat fluxes. A ''gust factor,'' in which the wind speed was assumed to have a minimum of 4 m s^{-1} for the heat flux and vertical mixing computations, represented the unresolved high-frequency wind events (including during the imposed MJO anomalies described below).

The present experiment was conducted by comparing two parallel runs of the OGCM: one forced entirely with climatological annual cycle wind stress (denoted τ_{CLIM}), and the other with climatological winds plus idealized intraseasonal anomalies meant to correspond to MJO winds. In each case the model was first spun up for 3 years with annual cycle winds. (Experiments with longer spinup times showed that initialization transients were not contaminating the solutions for the present purposes.) At the start of year 4 the two runs diverged: the ''control run'' simply continued the climatological forcing, while the ''MJO run'' added intraseasonally oscillating zonal wind stresses on top of the climatology in the western equatorial Pacific. The idealized MJO winds were defined to be purely sinusoidal with equal-amplitude easterly and westerly phases; therefore, they did not change the low-frequency wind stress climatology. It is not suggested that the real MJO winds always have this character; rather, the point of this idealized experiment is to isolate the possible rectification, aside from any simultaneous changes in the low-frequency winds that occur during El Niño events. This tricky issue is further discussed in section 5. The idealized MJO wind

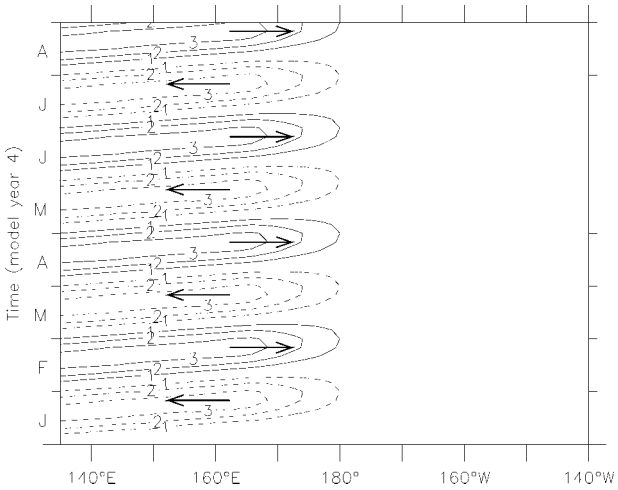

FIG. 2. The structure of the idealized MJO zonal wind stress anomalies along the equator during model year four. Line contours show eastward winds, dashed contours westward winds, with contours at ± 1, 2, and 3×10^{-2} N m^{-2}. The arrows are simply a visual aid to show the direction of each phase of the wind. The winds are described by Eqs. (1)–(3), and represent eastward-advancing oscillations. East of the anomaly region, the forcing remained climatological.

anomalies had the following characteristics: Gaussian about the equator; sinusoidal in x and t, with phase advancing eastward; at the eastern edge of the MJO region the anomalies ramped down to zero so winds remained climatological in the east. These wind stress anomalies $\tau^x_{\rm MJO}$ were specified as the product of a function of (x, t) times a function of y:

$$\tau^x_{\rm MJO} = Af(x, t)g(y), \tag{1}$$

where A is the wind stress magnitude (3.5×10^{-2} N m^{-2}), and the functions $f(x, t)$ and $g(y)$ are

$$f(x, t) = R(x) \sin\left(2\pi \frac{x - c_m t}{c_m T}\right), \qquad g(y) = e^{-(y/Y)^2} \tag{2}$$

where c_m is the eastward advancement speed of the oscillation (5 m s^{-1}), T is the period of the oscillating winds (60 days), and Y is the meridional scale of the Gaussian (6° latitude). These values of speed and period imply a zonal wavelength for the MJO of about 230° longitude. The parameter values are based qualitatively on observations; relevant observations and experiments to test the sensitivity of the model solutions to these choices are discussed in section 3c. The linear ramp $R(x)$ that defines the east edge of the MJO forcing winds is

$$R(x) = \begin{cases} 1 & \text{for } x \text{ west of } 165°\text{E} \\ 0 & \text{for } x \text{ east of } 175°\text{W} \\ (175°\text{W} - x)/20 & \text{for } 165°\text{E} < x < 175°\text{W}. \end{cases} \tag{3}$$

The time–longitude structure of these idealized winds is shown in Fig. 2.

The wind stress anomalies $\tau^x_{\rm MJO}$ were added directly to the climatological zonal stresses $\tau^x_{\rm CLIM}$ (i.e., $\tau^x = \tau^x_{\rm CLIM} + \tau^x_{\rm MJO}$), although such addition is not strictly consistent, since a change in the zonal wind component affects the wind speed and therefore would also modify the background stresses $\tau_{\rm CLIM}$. The correct way to perform this addition would be to add anomalies of zonal wind component to the climatological zonal wind, then recompute the total wind speed, then use that value to recompute both components of wind stress. We chose not to do this since we wish to compare two model runs with identical wind stresses averaged over one period of the intraseasonal anomalies; a correct wind component addition would change this low-frequency mean stress (the low-frequency change would be easterly in regions and times where $\tau^x_{\rm CLIM}$ was easterly, and westerly where $\tau^x_{\rm CLIM}$ was westerly). Such changes to the background stress would make it difficult to isolate and interpret the fairly subtle intraseasonal processes discussed here.

The imposed MJO forcing acted on the model both through the dynamics (wind stresses) and thermodynamics (wind speed). Wind speed affects the model through evaporation and through stirring and consequent changes of mixed-layer depth. For these purposes wind speed is calculated from the imposed total stresses by

$$|\mathbf{u}| = \frac{(\tau^{x^2} + \tau^{y^2})^{1/4}}{(\rho_a c_D)^{1/2}}. \tag{4}$$

To further decipher some aspects of the results, a third parallel model run was made in which MJO wind stress anomalies given by (1)–(3) were imposed, but the anomalies acted only on the dynamics, while the wind speed remained climatological [i.e., (4) was evaluated only with $\tau_{\rm CLIM}$]. Thus in this run the evaporation and vertical mixing remained unaffected by the MJO winds. This experiment is referred to here as the ''stress-only'' run.

Although the convection-favorable phase of the MJO is associated with increased cloudiness, in the present paper, no effects of changes in solar radiation due to clouds are considered. Parallel model experiments with cloud anomalies similar in form to the winds showed that idealized MJO cloud variations did not produce a significant rectified signal. Of course the cloud fluctuations did induce an SST oscillation, but not a low-frequency SST change in these experiments. It may very well be, however, that coupled intraseasonal feedbacks could occur in reality associated with SST–convection interactions that are not simulated in the present uncoupled context (e.g., Flatau et al. 1997).

b. Intermediate coupled model

To evaluate the effects on the coupled system of rectified signals found in the OGCM, an intermediate anomaly model was used, comparable in complexity to the model of Zebiak and Cane (1987). It retains only those physical processes of the ocean and atmosphere thought responsible for the large-scale, low-frequency

behavior of the tropical Pacific. The model is described in detail elsewhere (Kleeman 1993; Kleeman et al. 1992) and here we provide a relevant summary: The atmospheric component is steady-state and produces a unique (since the atmosphere has no internal variability) response to a given SST anomaly pattern. The dynamics are as described by Gill (1980) while a simplified convection scheme (Kleeman 1991) allows for the realistic depiction of midtropospheric latent heating. This model, unlike the Zebiak and Cane (1987) formulation, responds very nonlinearly to SST anomalies in that a high background SST field is required to obtain a significant dynamical response.

The ocean model dynamics consists of a prognostic shallow water equation set which is forced by wind stress anomalies. These equations assume the long wave approximation and for computational efficiency retain only the first six equatorial Rossby modes. The ocean model prognostic SST equation allows only for the influence of thermocline perturbations (that is, there is no horizontal SST advection) and has a Newtonian damping term.

Coupling is achieved by the exchange of SST anomaly (produced by the ocean) and wind stress anomaly (produced by the atmosphere). This model has been used operationally to predict ENSO at the Australian Bureau of Meteorology for the past four years. It has historical and real-time levels of skill that compare favorably with other routine ENSO prediction systems (Kleeman 1999), some of which are considerably more physically detailed. This suggests that it depicts the dominant modes of ENSO behavior realistically.

In the experiments described below, the model was initialized to 1 January 1997 using historical wind and subsurface data. These data were assimilated into the model ocean using a space–time variational method (Kleeman et al. 1995). As in the case of the OGCM, two parallel runs were made: a control run that ran freely following initialization, and a run designed to simulate the rectified SST effects seen in the OGCM, described in section 3b below.

c. *Observational data used for comparison*

In several sections, observations from the TAO array of temperature and surface meteorology moorings (Hayes et al. 1991; McPhaden 1993) are used to interpret model results. The TAO array consists of nearly 70 moorings arranged in pickets nominally 15° longitude apart across the equatorial Pacific. Each picket has moorings at the equator, ±2°, ±5°, and ±8° latitude, most of which are thermistor chain moorings that measure temperature at 1-m depth and 10 subsurface depths down to 500 m, as well as surface winds, relative humidity, and air temperature. At 0°, 165°E (and at three other longitudes) an enhanced mooring also measures zonal and meridional currents between the surface and 300m; these are a combination of mechanical current meters and downward-looking acoustic doppler current profilers (ADCPs). Kessler et al. (1996) discuss statistical and sampling error characteristics of the TAO buoy network.

3. Results from the OGCM forced by idealized MJO wind stresses

As detailed in section 2a, following a 3-yr spinup with climatological winds, two parallel runs of the OGCM were made: a control run that continued the climatological annual cycle forcing, and a run in which idealized MJO wind stress anomalies were added on top of the climatology in the western equatorial Pacific. The MJO anomalies had equal-amplitude easterly and westerly phases so the low-frequency wind stress forcing of the two runs was the same. The effects of MJOs are evaluated by comparing the two runs during year four. Difference fields between these two runs are taken to be the effect of the MJO on the model ocean.

a. *Model temperature and current differences due to MJO winds*

Figure 3 shows the difference in SST and surface zonal current along the equator during year four between the run with idealized MJO winds imposed on top of climatology and the run with climatology alone. The top panels show the unsmoothed differences, while the bottom are a 60-day running mean to remove the intraseasonal fluctuations. The smoothed difference fields can be interpreted as the rectified signature of the MJO wind anomalies in the OGCM.

Consider first the zonal current effects (right, Fig. 3). The OGCM response to the initial MJO episode in the early months of year four appears roughly as would be expected from linear dynamics: easterly winds spin up a westward current, then westerly winds spin up an eastward current (Fig. 3, top right). These signals propagate east of the forcing region at close to the model first baroclinic mode Kelvin wave speed (about 3 m s^{-1}; see section 3.3 of Moore et al. 1998). However, by the second MJO cycle, the oscillation is overshadowed by a lower-frequency eastward surface current anomaly, and this eastward trend continues through subsequent cycles (note the trend to red shading in Fig. 3, top right). Figure 4 shows the surface current difference averaged over year four in plan view. Under the oscillating winds in the western equatorial Pacific, a mean eastward surface jet has been generated, and the eastward tendency extends all the way to the eastern boundary, within about ±2° latitude. On both sides of the equator, but especially in the Northern Hemisphere, surface current differences are generally westward. The magnitude of these rectified currents is about 15–20 cm s^{-1} under the strong winds and up to 5 cm s^{-1} outside the anomalous wind region, not a small fraction of the climatological flows, partic-

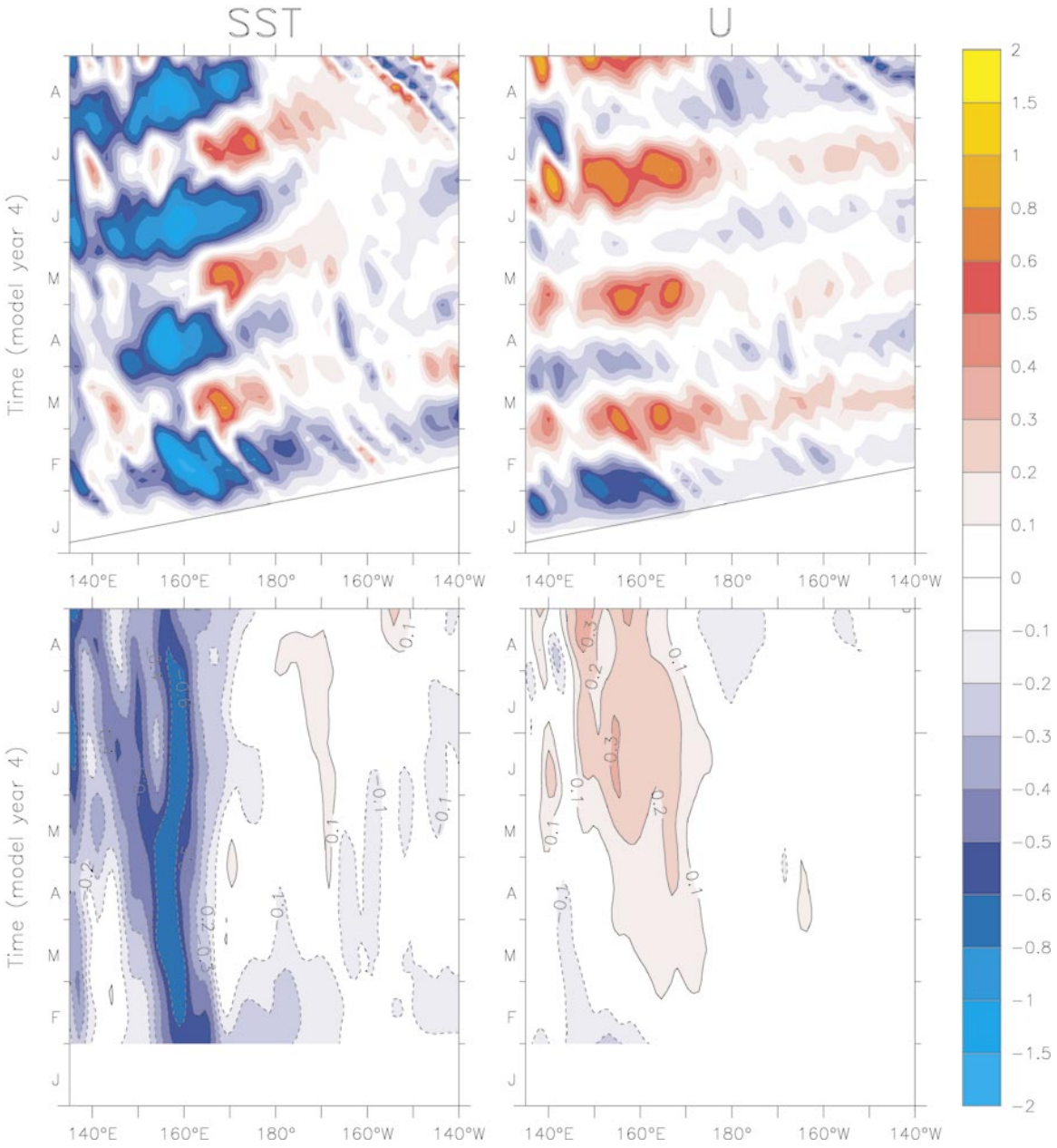

FIG. 3. SST and surface zonal current differences along the equator due to oscillating MJO winds. In each case the fields plotted are the difference, during model year 4, between the run with added MJO winds and the control run with climatological winds. (left) SST; (right) zonal current. (top) unsmoothed; (bottom) 60-day running means. The scale for all fields is at right (°C for SST; m s^{-1} for zonal current). The overlaid slant lines at the top show the first baroclinic mode Kelvin wave speed for the model stratification (3 m s^{-1}).

ularly on the equator where the South Equatorial Current is weak.

SST differences (Fig. 3, left panels) also demonstrate low-frequency changes in addition to the intraseasonal oscillation. Under the strongest MJO winds (west of about 170°E), SST cools during each easterly wind period and warms under the westerlies, as might be expected due to equatorial upwelling, with an amplitude of about ±0.5°C. However, the cooling is larger, resulting in a net rectified SST drop of about 0.4°C compared to the climatological run, within a couple of MJO cycles (Fig. 3, bottom left). East of the strong wind region, SST also oscillates intraseasonally, and these signals are seen to progress eastward at a slightly slower speed than the Kelvin wave (Fig. 3, top left). The low-frequency SST change in this eastern region is, in contrast to the cooling in the west, a net rise of a tenth of a degree or so compared to the climatological run.

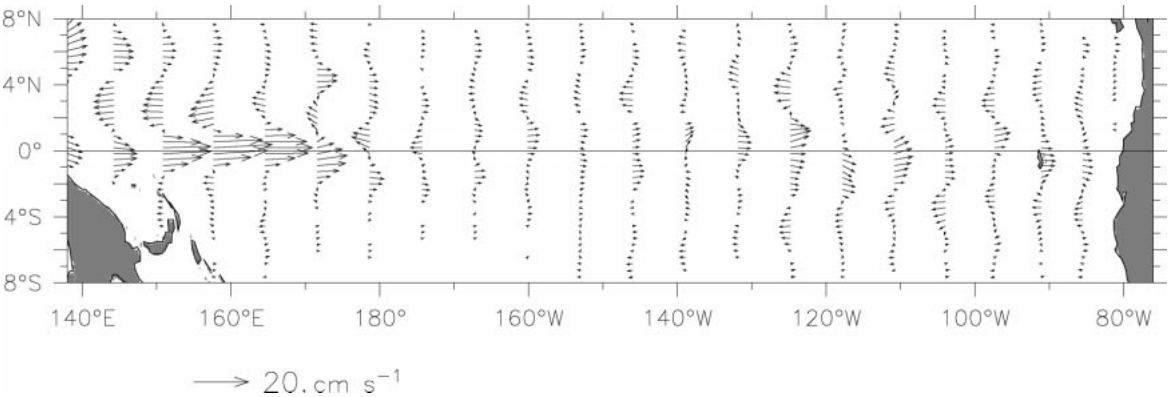

FIG. 4. Mean surface current difference due to MJOs: the difference between the MJO and the climatological control runs, averaged over four MJO cycles.

b. Rectifying processes in the OGCM

In this section, the mechanisms producing the changes in zonal currents and SST noted in section 3a are diagnosed. Three main processes were noted, all of which act in the sense to cool the far western Pacific and warm the central Pacific.

1) EVAPORATIVE COOLING

Latent heat flux is evaluated in the OGCM according to standard bulk formulas, assuming that humidity is a fixed proportion (0.78) of the saturation humidity at the model SST (Seager et al. 1988). Latent heat flux is thus taken to be a function of wind speed and SST. This choice is reasonable since humidity varies over a relatively small range in the west Pacific warm pool (in the more than 6 yr of humidity record at the TAO mooring at 0°, 165°E the rms of daily-average relative humidity was 4.4% about a mean of 78%) and its fluctuations are apparently a second-order influence on evaporation in this region. Variations of wind speed are far more important (Shinoda et al. 1998; Hendon and Liebmann 1990).

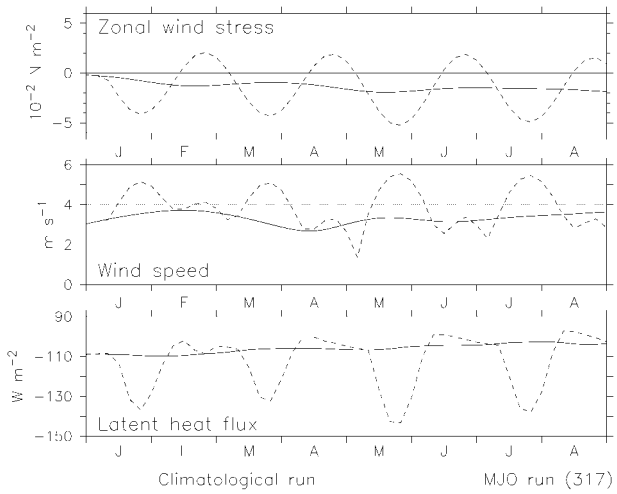

FIG. 5. Zonal wind stress, wind speed, and latent heat flux at the equator, 150°–170°E, comparing the climatological control run (solid line) and the MJO run (dashed line). (top) zonal wind stress (10^{-2}N m^{-2}); (middle) wind speed (m s^{-1}) [the dotted line at 4 m s^{-1} shows the value of the model's gust factor, see section 3b(1)]; (bottom) Latent heat flux (W m^{-2}, with negative values indicating heat loss by the ocean).

It has been noted that the active-convection phase of the MJO is associated with strong wind events on a variety of time- and space scales, including local storms and squall lines as well as the intraseasonal westerlies, while the anticonvection phase can be characterized by moderate, but relatively steadier, trade winds. The question of accounting for the effect of high-frequency, small spatial-scale winds on evaporation and mixing has not been satisfactorily answered, either for models or low-resolution observations, and we follow the common practice in ocean modeling of specifying a gust factor, in which the wind speed is assumed never to go below 4 m s^{-1}. This choice has a large effect in the warm pool region where climatological monthly winds are typically 1–2 m s^{-1} (each component). In the present study, the climatological wind speed used to force the control run never goes above 4 m s^{-1} in the warm pool region, so the control run latent heat fluxes are always based on the gust factor minimum (Fig. 5, middle). The imposed MJO wind stresses produce speeds usually larger than the climatological winds during peaks of both signs. This results in a 30-day periodicity for the wind speed and a mean latent heat flux cooling tendency about 5–10 W m^{-2} larger than that in the climatological run (Fig. 6, top). Another measure of the magnitude of this intraseasonal evaporation effect on model SST can be estimated by comparing the MJO run with the stress-only run in which the idealized MJO anomalies were not allowed to modify the wind speed, but forced the model only through the dynamics (see section 2a). In the stress-only run, the roughly 0.4°C low-frequency cooling compared to the climatological run seen in Fig. 3 (bottom left) was reduced by about half.

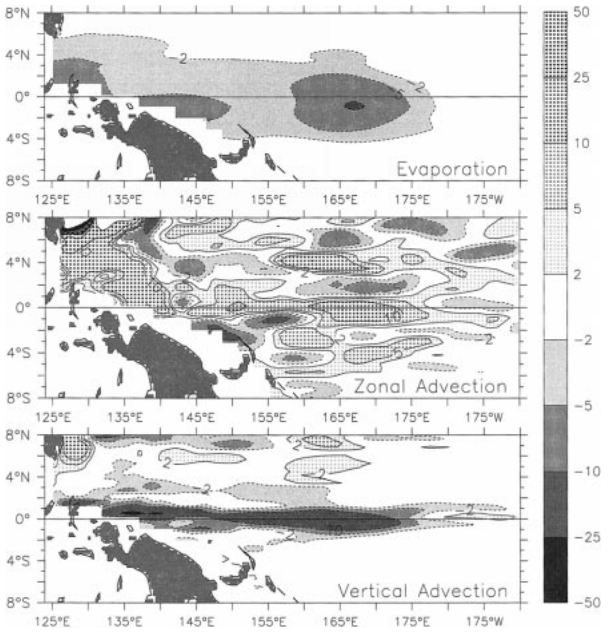

FIG. 6. Mean heat flux difference terms (the difference between the MJO and the climatological control runs) averaged over four MJO cycles (W m^{-2}). (top) Latent heat flux; (middle) zonal advection heat flux; (bottom) vertical advection heat flux. Negative values (cooling the ocean) are shaded; positive values are hatched.

2) NONLINEAR ZONAL CURRENT FORCED BY OSCILLATING ZONAL WINDS

Figures 3 and 4 document that the purely oscillating zonal wind stress anomalies of the MJO run produced a net eastward current on the equator, and westward current off the equator, most strongly at the longitudes of the imposed winds, but also extending well eastward. Robinson (1966; also see Gill 1975) showed that the first-order nonlinear effect on equatorial zonal currents is eastward, whatever the sign of the wind. This effect is due to the Ekman divergence associated with equatorial zonal winds. Easterly winds directly force a westward surface current, but also cause Ekman divergence that advects the westward momentum away from the equator, resulting in an eastward advective contribution at the equator, and corresponding westward term off the equator. Westerly winds, on the other hand, directly force a surface eastward current, but also produce Ekman convergence, concentrating the eastward momentum on the equator. Thus both signs of zonal winds produce an eastward nonlinear modification at the equator, a westward modification off the equator, and the result is the pattern of current differences seen in Fig. 4. These nonlinear eastward equatorial currents produce the rectified warming seen to the east of the strong wind region (near 170°W) in Fig. 3 (left panels), through zonal advection of the background SST gradient. Note that the intraseasonal SST oscillations east of the strong wind region propagate eastward at a speed less than that of the Kelvin wave (Fig. 3, top left), consistent with an advective rather than a wave process.

In addition to the SST advection due to the rectified current itself, there is a further rectification due to the intraseasonal correlation between u and dT/dx. For the intraseasonal variation, the eastward current phase occurs under westerly MJO winds and hence warmest SST in the west. Therefore the zonal SST gradient at this time is more strongly negative than climatology and zonal advection is an anomalous warming term. Conversely, in the easterly phase, SST under the imposed MJO winds is cooler, therefore the zonal SST gradient is weaker than average, and the westward currents that would be expected to be cooling have reduced effect. Thus the term udT/dx anomalously warms the region at the east edge of the MJO winds through both the oscillating and low-frequency elements. That is, if u' is the oscillating (intraseasonal) and u'' the nonlinear (low-frequency) zonal current, and T' the intraseasonal and $\overline{T}$ the background temperature, both the terms $u'dT'/dx$ and $u''d\overline{T}/dx$ are negative (since $d\overline{T}/dx$ is negative). Therefore zonal advection warms SST under and to the east of the MJO wind region due to both processes. The magnitude of the rectified warming, averaged over four MJO cycles is about 10 W m^{-2} (Fig. 6, middle).

3) CHANGES IN VERTICAL PROFILES OF TEMPERATURE AND ZONAL CURRENT

A third nonlinear process due to the idealized MJO wind forcing contributes to cooling the west Pacific through covariation of the vertical temperature gradient and upwelling, and depends on the relation between the 60-day period of forcing and the spinup time of the equatorial currents. In a linear model in which upwelling fluctuations due to oscillating zonal winds acted on a constant background vertical temperature gradient, vertical advection of temperature due to oscillating upwelling would cancel over one cycle, but in the OGCM other processes combine to make vertical velocity w' positively correlated with dT'/dz and there is a net cooling.

When a zonal wind anomaly is imposed on the equator, a surface downwind current is forced, and in addition an opposing pressure gradient is also generated. This pressure gradient accelerates an undercurrent that is directed opposite to the surface current. In the model the spinup time for the surface current is about 8–10 days behind the wind, while for the undercurrent the lag is about 10–15 days, in agreement with observations (see appendix B). Since the zonal temperature gradients are in the same sense at both the surface and subsurface, this pattern of current alternately strengthens the vertical temperature gradient (following the westerly phase in which zonal advection anomalously warms the surface and cools the subsurface) and weakens it (following the easterly phase). The maximum temperature anomalies induced by these advective heating and cooling signals

further lag the currents by about one-quarter period (15 days). The result of these lags is that the vertical temperature gradient is largest about 25–30 days following the maximum westerly winds, that is, almost at the time of maximum easterly winds, and correspondingly weakest at the time of maximum westerly winds. Since upwelling w' is directly forced by Ekman pumping it is nearly in phase with the winds, therefore maximum upwelling occurs at the time of maximum vertical temperature gradient and cools the surface more than would be expected based on the background gradient.

The vertical advection mean difference was tightly confined to the equator with a magnitude of about 15 W m^{-2} (Fig. 6, bottom). The effect on SST was estimated by comparison with the parallel stress-only model run in which the MJO wind stresses were allowed to force the model ocean only through the dynamics, which removed the effect of evaporation so most of the cooling was due to the interaction of w' and dT'/dz described here. The comparison suggested that on the equator the magnitude of this influence on SST was about as large as that due to evaporation. However, since equatorial upwelling has a narrow meridional scale (about 1° latitude in this model), the vertical-advection-induced SST effect was more equatorially trapped than that due to evaporation, which does not depend on equatorial dynamics and had a scale more like that of the strong MJO winds themselves (3°–4° latitude). Therefore the overall impact of the evaporative changes was more important.

c. *Model tests of the sensitivity to parameter choices and the form of the wind*

Observed intraseasonal variability is relatively broadband and contains both coherent eastward-propagating components like those modeled by (2), and smaller spatial-scale features that may propagate in any direction. Therefore it is important to determine whether the OGCM results shown in Figs. 3–6 are sensitive to the values chosen for wind stress amplitude, eastward propagation speed and period, or to the large spatial scale of the idealized forcing functions. The purpose of these experiments was to evaluate whether the model results are likely to be a robust representation of the effects of actual broadband intraseasonal variability on the ocean or are due to peculiarities of the idealized and therefore unrealistic choices made here. We investigated these sensitivities through a series of model runs with varying forcing properties.

1) MJO-FORCING PARAMETERS

The first series of tests varied the parameters A, c_m, and T (wind stress amplitude, MJO eastward propagation speed and period, respectively) that describe the idealized forcing functions in Eqs. (1) and (2). The model setup was otherwise exactly as described in section 2a. As a simple measure for the effect of the parameter variations, we use SST difference from climatology averaged over the equatorial warm pool region (1°S–1°N, 150°–170°E), and over three MJO cycles, denoted SST_{av} (inspection of the complete fields suggested that this was a reasonable metric for the overall rectified SST signature).

The value chosen for wind stress amplitude A in the main MJO run was 3.5×10^{-2} N m^{-2}; we tested values ranging from 2 to 6×10^{-2} N m^{-2}. Shinoda et al (1998) used ECMWF winds to estimate a peak-to-peak composite MJO wind stress as 5×10^{-2} N m^{-2} (about 30% smaller than our choice), while individual events seen in the TAO moorings were up to twice as large (Cronin and McPhaden 1997; Ralph et al. 1997). In the model experiments varying the forcing amplitude, SST_{av} cooled roughly linearly with increasing wind stress, about 0.1°C for every 1×10^{-2} N m^{-2} increase in wind stress. In general, the nonlinear effects [especially the nonlinear eastward current discussed in section 3b(2)] became smaller as the wind forcing became smaller. Therefore the weak warming near the date line, due to eastward advection by this current, was more sensitive to the forcing amplitude than was SST cooling farther west (due substantially to evaporation, which depends on the square root of wind stress and therefore varies less than forcing amplitude). These sensitivities to forcing amplitude suggest that it takes a moderate or larger intraseasonal event (winds of 3×10^{-2} N m^{-2} or stronger) to produce a significant rectified interaction with the coupled system.

It is also worth noting that the magnitude of the SST cooling in the OGCM was comparable to those observed during strong MJO events. The peak-to-peak intraseasonal SST oscillations were 1°–1.5°C (the intraseasonal rms was about 0.5°C). This is larger than composite MJO SST (Shinoda et al. 1998 found composite SST oscillations of about 0.5°C) but similar to observed intraseasonal SST signals during the moderate MJO events of the Tropical Ocean and Global Atmosphere Coupled Ocean–Atmosphere Response Experiment (TOGA COARE) intensive observation period in 1992–93 (Ralph et al. 1997; Cronin and McPhaden 1997).

The second parameter, MJO propagation speed c_m, was chosen to be 5 m s^{-1}; we tested speeds ranging from 2.75 to 10 m s^{-1}, which span the range of reported values (Shinoda et al. 1998; Rui and Wang 1990). MJO propagation speed could potentially affect the solution since eastward-moving wind forcing projects more strongly onto the Kelvin mode if its speed is near the oceanic first baroclinic mode Kelvin wave speed (about 3 m s^{-1}; Weisberg and Tang 1983). However, the projection enhancement is significant only when the zonal fetch of the propagating forcing is long; in this case the zonal extent of the idealized MJO winds is only 40° longitude, which is too short to have much of an effect. For this reason we found little difference in the OGCM intraseasonal Kelvin waves due to this range of c_m, and virtually no difference in the resulting rectified SST. In

addition, most of the rectifying effects seen in these runs are essentially local processes, so the MJO propagation speed is not a critical factor in this situation.

The third parameter that defined the idealized MJO winds is the period *T.* Observed MJO periods range from about 30 to 70 days with a broad peak near 50–60 days (Hendon et al. 1999); we chose the value 60 days for the main MJO run, but tested periods ranging from 20 to 120 days. In general, there was a roughly linear increase in the rectified SST cooling signature SST_{av} as the period increased, from about 0.15°C at 30-day periods to 0.3° at 60-day periods to 0.5°C at 90-day periods. Changes in SST_{av} flattened out in runs with periods shorter than 30 days or longer than 90 days. It is not known what determines the model sensitivity to MJO period, but the effects were seen in all three advection terms, and apparently represented a complicated interaction between the spinup times for various aspects of the equatorial circulation and the temperature gradients resulting from advection. As the delicacy of the phase relations between vertical velocity and temperature gradient [section 3b(3)] illustrates, these interactions can become quite complex. However, the results do show that the rectification occurs throughout the intraseasonal band. Overall, the exercise of varying the MJO parameters A, c_m, and T indicates that the SST changes shown in Figs. 3–6 and discussed in section 3b are a robust response in this OGCM to reasonable choices of parameters to describe the MJO.

2) SINUSOIDAL TEMPORAL STRUCTURE OF THE MJO FORCING

A second set of model runs was intended to examine the implications of our choice of a sinusoidal form for the MJO anomalies [Eq. (2); Fig. 2]. In reality, intraseasonal wind variations do not have equal and parallel positive and negative phases; often the westerly phase is characterized by higher wind speeds than the easterly (Cronin and McPhaden 1997). However, our choice was made in order to isolate the question of rectification without the complication of the general shift to low-frequency westerlies that is often observed during the onset of El Niño. Our assumption of stronger than normal easterlies as well as westerlies is particularly significant in regards to the importance of evaporation, which was a cooling term during both phases of the anomalous wind, since the background climatological winds over the west Pacific warm pool are very weak. Some observations [e.g., Cronin and McPhaden (1997), working with the 4-month TOGA COARE time series, and Hendon and Glick (1997), working with European Centre for Medium-Range Weather Forecasts atmospheric reanalysis fields] show that at least in some periods the anticonvection (easterly) phase of the MJO is instead associated with generally low wind speeds, which would imply weak evaporation and contradict that aspect of the rectification found in the present experiments. However, even if this alternate scenario is a more accurate description, these studies suggest that an active MJO period represents anomalously strong overall winds and evaporative cooling, relative to climatology, so net cooling during a full cycle should still occur. M. F. Cronin (1998, personal communication) points out that west of about 160°E the anticonvection phase usually has quiet winds with only occasional easterlies, while east of this longitude MJO westerlies occur as an episodic interruption of trade winds; therefore our assumption of strong winds in both phases may be most appropriate only to the region east of 160°E. This is a difficult question to evaluate from existing observations, because it is not straightforward to statistically extract the evaporation signal of the MJO, since its highest wind speeds occur at many time- and space scales, including local storms and squall lines that are associated with the convection phase of the MJO but have much smaller scales than it. Therefore bandpass filtering to intraseasonal frequencies can remove much of the evaporative signal. We examined many individual events in hourly time series of winds from TAO moorings in this region, and found examples of events with high wind speeds in both phases as assumed here, and also examples in which the anticonvection phase had quiet winds; overall it was not possible to make a compelling characterization either way from the existing sparse data.

To test the OGCM response to this aspect of the variability, the original sinusoidal wind stresses were replaced by a time series of Gaussian humps composed of relatively short-lived but strong westerlies and longer-lasting but weaker easterly phases (the mean was still zero). For the same rms wind stress amplitude, the Gaussian hump winds produced weaker SST anomalies (by about 20%) than the sinusoidal winds, mostly because of reduced evaporation during the weak easterly phase. However, the qualitative response of cooling under the strong forcing and slight warming to the east remained similar to that of the sinusoidal winds.

It was noted in section 2a that in order to isolate the effects of intraseasonal forcing without the complication of changing the low-frequency stress, we specified wind stress anomalies τ^x_{MJO} rather than the wind itself. The effect of adding oscillating zero mean wind component anomalies would have been to increase the wind speed averaged over one cycle and thereby change the low-frequency total stresses (both components). This change would be easterly where τ^x_{CLIM} was easterly and westerly where τ^x_{CLIM} was westerly. Since the real MJO winds occur typically in October–March when the climatological background over the western Pacific is westerly, the wind speed increase due to the oscillating part alone of the MJO should preferentially favor increasing the westerly stress forcing of the ocean. Our procedure of adding stresses should therefore be an underestimate of the real effect of MJO winds on the western Pacific.

3) Spatial coherence of the MJO forcing

A final series of model runs tested the difference between the effects of the coherent MJO and those of the smaller spatial-scale intraseasonal variations, which make up about half the total intraseasonal variance in this region (Hendon et al. 1999). To model the incoherent intraseasonal signals, an SVD decomposition (Bretherton et al. 1992) of bandpassed OLR and the same field phase-shifted one-quarter period was done (e.g., Zhang and Hendon 1997); the first two eigenvectors of which were a quadrature pair that described a coherent, eastward-propagating MJO mode, similar to mode pairs extracted by various EOF-based techniques (e.g., Hendon et al. 1999). The third and fourth eigenvectors also stood out as a pair, but higher modes were apparently noisy with gradually decaying eigenvalues. Eigenvectors 5–14 were taken as representative of the spatial scales of incoherent intraseasonal variability and used to construct wind fields that had intraseasonal timescales but much shorter spatial scales (typically 1–2000 km in both the zonal and meridional directions). These ten fields were propagated both east and west in varying combinations and at varying speeds to produce five realizations of incoherent intraseasonal forcing with the same amplitude as the sinusoidal wind stresses of the main MJO run [still multiplied by the meridional Gaussian according to the second of Eqs. (2) and ramped on the eastern edge according to (3)]. Perhaps surprisingly, the rectified SST fields resulting from these experiments were not so different from the coherent wind run; in particular each of the incoherent-forcing runs had the same character of cooling under the strong winds and weaker warming to the east. In general, evaporative cooling in these model runs had a similar effect as in the main run, but both the zonal and vertical advection terms were less efficient, apparently because of the incoherence of the wind forcing [note that these terms oppose each other in the heat balance (Fig. 6) and therefore reduction of both tends to cancel the difference]. It was also found that meridional advection became relatively more important in the heat balance, since the empirical spatial patterns included meridional gradients at the equator, which the sinusoidal forcing described in (2) did not contain. Nevertheless, the fact that the rectified SST signal remained qualitatively the same as under the spatially coherent, MJO-like winds indicate that the results reported here do not depend heavily on the form of the forcing, but that strong intraseasonal winds over the warm pool will always produce this pattern of rectified SST.

4. Coupled effects of the rectified SST

The sense of the rectified SST changes seen in the OGCM was to cool the western Pacific under the strong oscillating winds, and to slightly warm the region east of the direct forcing. From the point of view of the low-frequency coupled system, probably the most important effect is the consequent weakening of the zonal SST gradient, since that gradient is a major influence driving equatorial easterlies. The usual central Pacific SST gradient is about -0.5 to -1°C (1000 km)$^{-1}$, but the rectification induced in the OGCM by oscillating winds produced a much flatter SST region from about 155°E to 180°. We hypothesize that this SST gradient anomaly could feed back to the coupled system by weakening the background easterlies in this region and thereby enhancing the growth of El Niño.

To test this idea, an intermediate coupled model (section 2b) was used to compare two parallel experiments: a control run that ran freely following initialization to 1 January 1997 (just before the rapid growth of the 1997–98 El Niño), and a run designed to simulate the rectified SST changes found in the OGCM. Since the simplified dynamics and thermodynamics in this coupled model do not encompass the nonlinear processes noted to be important in the OGCM (section 3b), the oceanic effect of these processes was imposed externally. This imposed signal consisted of only the rectified (low-frequency) part of the OGCM SST. Intraseasonal variations themselves played no part in the coupled model experiments. The rectified SST was estimated as the net change in OGCM SST over four MJO cycles; that is the SST difference field over the 60 days centered on 31 August of model year 4 (Fig. 3), smoothed in *x*, *y*, and *t*. Values of this smoothed SST difference ranged from a cooling of up to -0.36°C (along the equator west of about 160°E) to a warming of 0.11°C near 1°N, 175°W. Coupled model SST was pushed toward this field for the first four months of 1997 by a strong Haney relaxation with a timescale of 1.74 days (Fig. 7, bottom). Except for this imposed forcing, the model ran freely in coupled mode, parallel to the coupled control run that was otherwise identical but without the externally imposed MJO SST.

Figure 7 compares the coupled control run hindcast of the 1997–98 El Niño (top) with the difference due to the hindcast with rectified MJO SST (bottom). The control run (top) predicted a weak warm event that raised SST in the eastern equatorial Pacific by a little more than 1°C, peaking in July–August 1997 and decaying at the end of the year. Anomalous westerly winds in this run were up to 1 m s^{-1} (Fig. 7, top). In common with several forecasts made at the end of 1996, the tendency toward a warm event in 1997 was clear but the magnitude was much too weak.

The externally imposed rectified MJO signal can be seen in the difference field as a cooling in the far west during January–April 1997, with weak warming near the date line (Fig. 7, bottom). The consequent weakening of the coupled model's zonal SST gradient produced additional westerly winds of about 0.5 m s^{-1}, blowing from the cooler west to the slightly warmer central Pacific, that strengthened the growing westerlies of the warm event (Fig. 7, bottom). This anomaly prop-

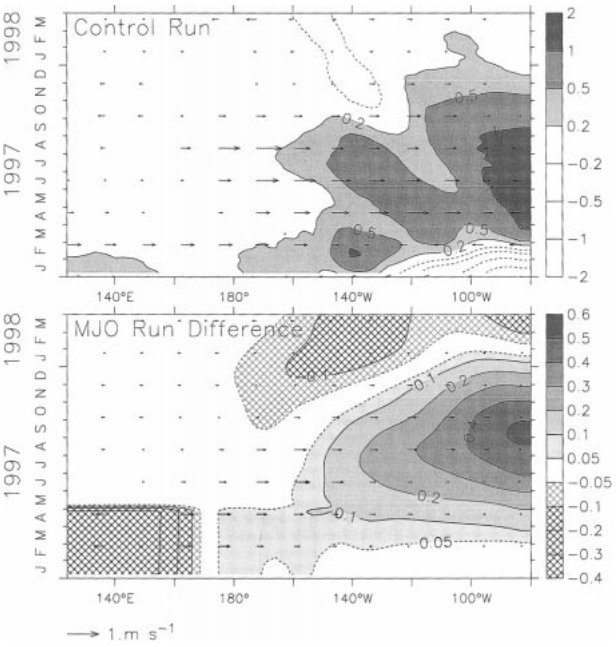

FIG. 7. SST (shading and contours) and zonal winds (vectors) on the equator during the coupled model runs. (top) control run hindcast initialized to 1 Jan 1997. (bottom) Difference between the control run and the run with the OGCM SST imposed. Note the different contour intervals in each panel.

agated eastward, with Kelvin waves deepening the thermocline to the east of the imposed cool SST and thereby producing warming in the central Pacific. This SST pattern generated additional westerly winds that continued and extended the eastward motion. Although Kelvin waves ensured that the propagation was eastward, the coupled SST–zonal wind anomaly propagated at about 1 m s^{-1}, much slower than the free Kelvin wave speed (Fig. 7, bottom). The net result was a coupled amplification of hindcast east Pacific SST at the height of the El Niño by more than 0.5°C, or about a 50% increase compared to the control run (Fig. 7, bottom).

The coupled model used here does not include the effects of zonal advection on SST as this was found to have little impact on model forecast skill (Kleeman 1993). Nevertheless, some authors (e.g., Picaut et al. 1997) have argued that zonal SST advection is important to the development of El Niño, so we repeated the experiment with this effect included (see Kleeman 1993 for details on how this is achieved). We found that the sensitivity shown in Fig. 7b was slightly enhanced but the results were qualitatively the same.

5. Summary and discussion

We have shown that an ocean general circulation model, forced with purely oscillating intraseasonal wind stresses similar to those observed during the Madden–Julian oscillation, developed rectified low-frequency anomalies in its SST and zonal currents, compared to a run in which the forcing was climatological. The rectification resulted from three main processes: first, evaporative cooling under strong winds of either sign [section 3b(1)]; second, an eastward equatorial current generated nonlinearly due to advection of wind input momentum by Ekman convergence/divergence [section 3b(2)]; and third, changes in the vertical temperature profile so that Ekman upwelling is correlated with the vertical temperature gradient and therefore produces a net cooling under oscillating winds (section 3b(3)].

The overall signature of the rectified anomalies in the OGCM was low-frequency SST cooling (about 0.4°C) in the western Pacific under the strong MJO winds due to both evaporation and vertical advection, and weaker warming (up to 0.1°C) in the central Pacific due to zonal advection acting on the background SST gradient (Fig. 3). One might expect that, in a coupled system, such a pattern of zonally contrasting SST anomalies (reducing or reversing the background SST gradient) would tend to spawn additional westerly wind anomalies as a result of SST-induced changes in the low-level zonal pressure gradient. This was tested in an intermediate coupled model initialized to 1 January 1997, preceding the 1997–98 El Niño. On its own, the model hindcasts a relatively weak warm event, but when the rectified SST pattern seen in the OGCM was imposed, the hindcast El Niño became about 50% stronger (measured by east Pacific SST anomalies, Fig. 7, bottom) as a coupled response did in fact produce the hypothesized additional westerlies.

A series of model runs examined the sensitivity of the OGCM rectification to intraseasonal forcing of various forms (section 3c). The relative importance of evaporation versus advection was qualitatively estimated by comparison with an additional OGCM run in which only the wind stress (not the speed) was modified by the oscillating high-frequency winds. This suggested that on the equator, the two processes produce about equal rectified SST changes in this model, although since evaporation is due to the wind directly, while advection is due to equatorial dynamics, evaporation in these experiments (and probably in reality as well) affected a wider meridional region and therefore was more important to SST overall. However, it is difficult to go beyond this qualitative assessment given the crudity of the idealized MJO winds and the weaknesses of the OGCM itself. Model runs exploring the parameter space defining the MJO (section 3c) showed that the SST rectification was insensitive to MJO propagation speed and produced similar patterns for all choices of forcing period within the intraseasonal band. Varying the amplitude of the stress forcing showed that the nonlinear terms (especially zonal advection) were much more effective at higher-stress amplitudes (larger than 3×10^{-2} N m^{-2}). On the other hand, evaporation depends on the square root of wind stress and therefore is less sensitive to the forcing amplitude. For these reasons the evaporative cooling under the strong winds is the most robust

feature of the rectification found in these experiments. Since 2–3 $\times 10^{-2}$ N m^{-2} is a typical value for the stress amplitude of the coherent, eastward-propagating part of the intraseasonal signal (Shinoda et al. 1998), this suggests that moderate or stronger MJO events should be sufficient to produce the effects noted here. Finally, it has been noted (e.g., Hendon et al. 1999) that perhaps half the intraseasonal variance over the west Pacific is spatially incoherent, often associated with the convection-favorable phase of the MJO but with smaller scales. Artificial small-scale intraseasonal wind fields were constructed to force the OGCM; the SST fields resulting from these runs had the same character of cooling under the strong winds in the west and weakly warming the central Pacific. Since the actual MJO occurrences over the west Pacific include both the coherent eastward-propagating mode and additional incoherent variability (both of which resulted in similar tendencies in the OGCM), a typical MJO should produce a significant rectified SST signature as found here. Overall, these model experiments suggest that the results are not qualitatively sensitive to the form of the forcing, but that strong intraseasonal winds over the warm pool will always produce this pattern of rectified SST.

The sensitivity of the coupled model used here to external perturbation of SST has been analyzed extensively elsewhere (Moore and Kleeman 1997; Kleeman and Moore 1997). This analysis shows that perturbations with spatial structures similar to those deduced here for the MJO (an east–west dipole along the equator) are particularly efficient in forcing a low-frequency ENSO response in this model. As other models have different optimal forcing patterns (e.g., Xue et al. 1997; Thompson 1998), the sensitivity of our results to the present simplified coupled model physics should be tested. A perhaps more convincing test of these ideas would be in a coupled GCM that simulated the full coupled interaction, including feedbacks at the intraseasonal timescale itself, which are known to occur in nature (Hendon and Glick 1997; Shinoda et al. 1998). A further aspect of the interaction of the MJO with ENSO that could be tested in a coupled GCM is that in reality the entire envelope of enhanced intraseasonal variance moves east with an advancing El Niño (Fink and Speth 1997; McPhaden 1999). Our results suggest that the rectifying SST and consequent westerly winds should also move east, amplifying the signal. Possible effects of this coupled propagation could not be studied by the present two-model, two-separate-calculation combination, but could in a coupled GCM.

The question of rectification of the MJO into the ENSO cycle is relevant to our ability to forecast El Niño events, since increased intraseasonal variability over the western Pacific has been a prominent feature of all the events since we have had the capability to observe these frequencies (with the introduction of satellite OLR in 1979; Fig. 1). If rectification of the MJO resulting in low-frequency SST changes does occur in nature, and if the result of these SST changes is a corresponding enhancement of westerly winds, then the amplification of warm events due to the MJO would need to be accounted for when making ENSO forecasts, which is presently not the case for at least some dynamical model forecasts. However, since the occurrence of individual MJOs is apparently weatherlike and not predictable far in advance, this suggests that it may be difficult to improve our ability to estimate the amplitude of foreseen oncoming El Niños, as was the case in 1997. In general, models that do not well represent the MJO (many present atmospheric GCMs) may be expected to underpredict the amplitude of El Niños for this reason.

In late 1996, several forecast models (including the one used here) correctly predicted that 1997 would see the development of an El Niño event. Yet none of these models forecast the extremely steep rise of central and eastern Pacific SST that took place in March–July 1997, following the strong MJO events of December 1996 and March 1997 (CPC 1996), until the impacts of those events had been assimilated by the models. [After the fact, model hindcasts have been run that do indicate a steep SST rise in early 1997, but these experiments have not been diagnosed (D. Anderson 1998, personal communication).] This suggests that the MJO events played a role in the extreme and unpredicted growth of the 1997–98 El Niño. We hypothesize that SST warming in the central Pacific associated with the onset of El Niño allows MJO-associated winds and convection to extend farther out over the Pacific, even if the global MJO does not change. Thus MJO winds during the onset of El Niño can develop a long fetch and consequent large effect on the ocean dynamics and thermodynamics and can enhance the amplitude of the event through the processes discussed here. From this perspective, it is not the low global-wavenumber MJO mode that varies with the ENSO cycle (it does not), but its fetch over the Pacific. This resolves the apparent contradiction that MJO activity occurs every year but El Niño does not. However, it is emphasized that, although the present results suggest that the MJO can interact constructively with the onset of El Niño to amplify a developing warm event, the MJO on its own does not appear to be the *cause* of El Niño. This distinction must be made because coupled models without anything resembling the MJO generate ENSO-like behavior and have demonstrated forecast skill. Though it seems clear that the ENSO cycle would exist without the MJO, this premise does not in any way preclude a role for rectification of the MJO and coupled feedback leading to enhancement of El Niño events as suggested here.

We have shown plausible mechanisms by which oscillating winds associated with the MJO can produce significant nonlinear effects on SST. Whether or not the model solutions studied here are realistic in detail, the sense of these effects does not appear to be model dependent, and all point in the direction of flattening the west Pacific zonal SST gradient, and therefore, in the

direction of enhancing westerly wind anomalies as the SST anomalies feed back to the atmosphere.

The present results suggest that the relatively high-frequency signals of the MJO can interact constructively with the ENSO cycle through nonlinear ocean dynamics and latent heat fluxes producing rectified SST that feeds back to the coupled system. Therefore further work toward understanding these processes and the factors that contribute to variations of the MJO, especially the precursor conditions that affect their amplitude, may enhance our ability to predict the strength of oncoming El Niños.

Acknowledgments. The authors thank David Battisti, Meghan Cronin, Russ Davis, Harry Hendon, Mike McPhaden, Andy Moore, Dennis Moore, Klaus Weickmann, and Bob Weller for illuminating discussions. A reviewer provided us with the opportunity to reconsider these issues in detail for almost a year. Support for this work came from NOAA's Office of Global Programs via the Stanley P. Hayes Center (WSK).

APPENDIX A

Significance of Correlations

In this paper, several lag correlation statistics with confidence ranges are presented. The 95% confidence ranges for these were estimated according to the procedure in Kessler et al. (1996), based on estimating the degrees of freedom from the independence timescale of Davis (1976). A correlation coefficient r with n degrees of freedom, may be transformed to a variable z (''Fisher's z''), such that $r = \tanh(z)$, which is approximately normally distributed with standard deviation $\sigma_z = (n - 3)^{-1/2}$ (Panofsky and Brier 1968). For normally distributed correlations, Student's t-test is an appropriate test to reject the null hypothesis that the values are not significantly different from zero. In section 1, a lag correlation between 1-yr running mean SOI and OLR intraseasonal variance (Fig. 1) was cited. In this case the Davis (1976) independence timescale for the filtered variables was found to be 370 days, leading to the estimate of about 17.5 degrees of freedom for the 18-yr time series. The 95% confidence range on the lag correlation r (back-transformed from the normally distributed z) was found from a t-test table to be 0.48; therefore the 0.72 correlation cited in section 1 is significant above this level.

APPENDIX B

Phase Relation of Observed Intraseasonal Winds, Currents, and Pressure Gradients

In section 3b(3) it was shown that, in the OGCM, phase relations between intraseasonal zonal currents at the surface and subsurface advected the background temperature so as to alternately strengthen and weaken the vertical temperature gradient at the different levels. The result of this was that upwelling speed w was positively correlated with dT/dz and therefore vertical advection provided a net SST cooling, averaged over one cycle of the MJO. In this appendix, we briefly examine available observations to determine if this is the case in nature. In particular we would like to know what the phase relation is between intraseasonal zonal winds and the zonal pressure gradient and zonal currents (surface and subsurface).

The data studied come from the TAO buoy array (see section 2c) at the equator, 165°E and nearby locations. Primary measured quantities are the winds at 4-m height, surface, and subsurface temperature, and subsurface current measured by a downward-looking ADCP. The common period of these observations at 165°E was from March 1991 to December 1997. A few data gaps occurred during this period, the largest for about 4 months in early 1995. For almost two years of the record, currents above 30-m depth were missing, so the 30-m current was chosen as an indicator of ''surface'' current, while the 175-m current was chosen to represent the currents at thermocline level. The zonal pressure gradient was estimated from the centered difference of 20°C depth between buoys at 156°E and 180°. The derivative of 20°C depth (rather than dynamic height), was chosen as an indicator of zonal pressure gradient because the TAO moorings did not regularly measure salinity and the dynamic height calculation would have to be made with a mean temperature–salinity relation. Since salinity variability not well represented by the mean temperature–salinity has been noted to significantly affect such estimates of dynamic height from the TAO moorings in this region (Ji et al. 2000), 20°C depth was used instead. In fact, the two estimates of intraseasonal pressure gradients are highly correlated and either field leads to the same conclusion in this case.

All the fields were bandpass filtered with half-power limits of about 35–140 days to extract the intraseasonal signal, and lag correlations were found among them. The 95% confidence ranges were found as in appendix A. For these bandpassed time series, the independence timescales were typically 5–10 days, resulting in hundreds of degrees of freedom and 95% confidence ranges for the correlations of about 0.15. All correlations cited here are above this standard.

The results show lag relations similar to those noted in the OGCM. The highest lag correlation is given:

- Zonal wind led 30-m current by 7 days ($r = 0.53$)
- Zonal wind led the zonal pressure gradient by 15 days ($r = 0.42$)
- Zonal wind led (negative) 175-m current by 15 days ($r = -0.23$)
- Zonal pressure gradient was in phase with (negative) 175-m current ($r = -0.34$)
- 30-m current led (negative) 175-m current by 8 days ($r = -0.23$)

From these values we can conclude that the phase relation noted in the OGCM is a realistic representation of the observed intraseasonal changes in the vertical profile of zonal current and pressure gradient at 0°, 165°E. In particular, the sequence described in section 3b(3), in which zonal winds spin up a surface current with a lag of 8–10 days, and also a zonal pressure gradient and oppositely directed thermocline-level current with a lag of 15 days, is realistic.

REFERENCES

Bretherton, C. S., C. Smith, and J. M. Wallace, 1992: An intercomparison of methods for finding coupled patterns in climate data. *J. Climate,* **5,** 541–560.

Chen, D., A. J. Busalacchi, and L. M. Rothstein, 1994a: The roles of vertical mixing, solar radiation and wind stress in a model simulation of the sea surface temperature seasonal cycle in the tropical Pacific Ocean. *J. Geophys. Res.,* **99,** 20 345–20 359.

——, L. M. Rothstein, and A. J. Busalacchi, 1994b: A hybrid vertical mixing scheme and its application to tropical ocean models. *J. Phys. Oceanogr.,* **24,** 7725–7741.

CPC, 1996: *Climate Diagnostics Bulletin.* Vol. 96, No. 10, 78 pp.

Cronin, M. F., and M. J. McPhaden, 1997: The upper ocean heat balance in the western equatorial Pacific warm pool during September–December 1992. *J. Geophys. Res.,* **102,** 8533–8553.

Davis, R. E., 1976: Predictability of sea surface temperature and sea level pressure anomalies over the North Pacific Ocean. *J. Phys. Oceanogr.,* **6,** 249–266.

Emanuel, K. A., 1987: An air–sea interaction model of intraseasonal interactions in the Tropics. *J. Atmos. Sci.,* **44,** 2324–2335.

Fink, A., and P. Speth, 1997: Some potential forcing mechanisms of the year-to-year variability of the tropical convection and its intraseasonal (25–70-day) variability. *Int. J. Climatol.,* **17,** 1513–1534.

Flatau, M., P. J. Flatau, P. Phoebus, and P. P. Niiler, 1997: The feedback between equatorial convection and local radiative and evaporative processes: The implications for intraseasonal oscillations. *J. Atmos. Sci.,* **54,** 2373–2385.

Gent, P. R., and M. A. Cane, 1989: A reduced gravity, primitive equation model of the upper equatorial ocean. *J. Comput. Phys.,* **81,** 444–480.

Gill, A. E., 1975: Models of equatorial currents. *Proceedings Symposium on Numerical Models of Ocean Circulation,* National Academy of Science, 181–203.

——, 1980: Some simple solutions for heat-induced tropical circulation. *Quart. J. Roy. Meteor. Soc.,* **106,** 447–462.

Hayes, S. P., L. J. Mangum, J. Picaut, A. Sumi, and K. Takeuchi, 1991: TOGA-TAO: A moored array for real-time measurements in the tropical Pacific Ocean. *Bull. Amer. Meteor. Soc.,* **72,** 339–347.

Hendon, H. H., and B. Liebmann, 1990: The intraseasonal (30–50 day) oscillation of the Australian summer monsoon. *J. Atmos. Sci.,* **47,** 2909–2923.

——, and M. L. Salby, 1994: The life cycle of the Madden–Julian oscillation. *J. Atmos. Sci.,* **51,** 2225–2237.

——, and J. Glick, 1997: Intraseasonal air–sea interaction in the tropical Indian and Pacific Oceans. *J. Climate,* **10,** 647–661.

——, C. Zhang, and J. D. Glick, 1999: Interannual variation of the Madden–Julian Oscillation during austral summer. *J. Climate,* **12,** 2538–2550.

Ji, M., R. W. Reynolds, and D. Behringer, 2000: Use of TOPEX/Poseidon sea level data for ocean analyses and ENSO prediction: Some early results. *J. Climate,* **13,** 216–231.

Jones, C., D. E. Waliser, and C. Gautier, 1998: The influence of the Madden–Julian Oscillation on ocean surface heat fluxes and sea surface temperature. *J. Climate,* **11,** 1057–1072.

Kessler, W. S., 1999: Interannual variability of the subsurface high-salinity tongue south of the equator at 165°E. *J. Phys. Oceanogr.,* **29,** 2033–2049.

——, and M. J. McPhaden, 1995: The 1991–93 El Niño in the central Pacific. *Deep-Sea Res. II,* **42,** 295–333.

——, ——, and K. M. Weickmann, 1995: Forcing of intraseasonal Kelvin waves in the equatorial Pacific. *J. Geophys. Res.,* **100,** 10 613–10 631.

——, M. C. Spillane, M. J. McPhaden, and D. E. Harrison, 1996: Scales of variability in the equatorial Pacific inferred from the TAO buoy array. *J. Climate,* **9,** 2999–3024.

Kleeman, R., 1991: A simple model of the atmospheric response to ENSO sea surface temperature anomalies. *J. Atmos. Sci.,* **48,** 3–18.

——, 1993: On the dependence of hindcast skill on ocean thermodynamics in a coupled ocean–atmosphere model. *J. Climate,* **6,** 2012–2033.

——, 1999: Forecasts of tropical Pacific SST using a low-order coupled ocean–atmosphere dynamical model. *Experimental Long-Lead Forecast Bulletin.,* **8,** 5–8.

——, and A. M. Moore, 1997: A theory for the limitation of ENSO predictability due to stochastic atmospheric transients. *J. Atmos. Sci.,* **54,** 753–767.

——, M. Latif, and M. Fluegel, 1992: A hybrid coupled tropical atmosphere ocean model: Sensitivities and hindcast skill. MPI Rep. 76, 37 pp. [Available from Max Planck Institute fur Meteorologie, Bundesstrasse 55, D-20146 Hamburg, Germany.]

——, A. M. Moore, and N. R. Smith, 1995: Assimilation of subsurface thermal data into a simple ocean model for the initialization of an intermediate tropical coupled ocean–atmosphere forecast model. *Mon. Wea. Rev.,* **123,** 3103–3113.

Knutson, T. R., and K. M. Weickmann, 1987: 30–60 day atmospheric oscillations: Composite life cycles of convection and circulation anomalies. *Mon. Wea. Rev.,* **115,** 1407–1436.

Kraus, E. B., and J. S. Turner, 1967: A one-dimensional model of the seasonal thermocline, II: The general theory and its consequences. *Tellus,* **19,** 98–105.

Lau, K. M., L. Peng, C. H. Sui, and T. Nakazawa, 1989: Dynamics of super cloud clusters, westerly wind bursts, 30–60 day oscillations and ENSO: A unified view. *J. Meteor. Soc. Japan,* **67,** 205–219.

Levitus, S., 1982: *Climatological Atlas of the World Ocean.* NOAA Prof. Paper 13, 173 pp.

Madden, R. A. and P. R. Julian, 1972: Description of global-scale circulation cells in the Tropics with a 40–50 day period. *J. Atmos. Sci.,* **29,** 1109–1123.

——, and ——, 1994: Observations of the 40–50-day tropical oscillation—A review. *Mon. Wea. Rev.,* **122,** 814–837.

McPhaden, M. J., 1993: TOGA–TAO and the 1991–93 El Niño–Southern Oscillation. *Oceanography,* **6,** 36–44.

——, 1999: Genesis and evolution of the 1997–98 El Niño. *Science,* **283,** 950–954.

Moore, A. M., and R. Kleeman, 1997: The singular vectors of a coupled ocean–atmosphere model of ENSO. Part 2: Sensitivity studies and dynamical interpretation. *Quart. J. Roy. Meteor. Soc.,* **123,** 983–1006.

——, and ——, 1998: Stochastic forcing of ENSO by the intraseasonal oscillation. *J. Climate,* **12,** 1199–1220.

Moore, D. W., R. C. Kloosterziel, and W. S. Kessler, 1998: Evolution of mixed Rossby–gravity waves. *J. Geophys. Res.,* **103,** 5331–5346.

Murtugudde, R., and A. J. Busalacchi, 1998: Salinity effects in a tropical ocean model. *J. Geophys. Res.,* **103,** 3283–3300.

Neelin, J. D., I. M. Held, and K. H. Cook, 1987: Evaporation–wind feedback and low-frequency variability in the tropical atmosphere. *J. Atmos. Sci.,* **44,** 2341–2348.

Panofsky, H. A., and G. W. Brier, 1968: *Some Applications of Statistics to Meteorology.* University of Pennsylvania Press, 224 pp.

Philander, S. G. H., 1990: *El Niño, La Niña and the Southern Oscillation.* Academic Press, 292 pp.

Picaut, J., F. Masia, and Y. duPenhoat, 1997: An advective-reflective

conceptual model for the oscillatory nature of ENSO. *Science*, **277,** 663–666.
Price, J. F., R. A. Weller, and R. Pinkel, 1986: Diurnal cycling: Observations and models of the upper ocean response to diurnal heating cooling and wind mixing. *J. Geophys. Res.,* **91,** 8411–8427.
Ralph, E. A., K. Bi, P. P. Niiler, and Y. duPenhoat, 1997: A Lagrangian description of the western equatorial Pacific response to the wind burst of December 1992: Heat advection in the warm pool. *J. Climate,* **10,** 1706–1721.
Robinson, A. R., 1966: An investigation into the wind as the cause of the equatorial undercurrent. *J. Mar. Res.,* **24,** 179–204.
Rossow, W. B., and R. A. Schiffler, 1991: ISCCP cloud data products. *Bull. Amer. Meteor. Soc.,* **72,** 2–20.
Rui, H., and B. Wang, 1990: Development characteristics and dynamic structure of tropical intraseasonal convection anomalies. *J. Atmos. Sci.,* **47,** 357–379.
Seager, R., S. E. Zebiak, and M. A. Cane, 1988: A model of the tropical Pacific sea surface temperature climatology. *J. Geophys. Res.,* **93,** 1265–1280.
Shinoda, T., H. H. Hendon, and J. Glick, 1998: Intraseasonal variability of surface fluxes and sea surface temperature in the tropical western Pacific and Indian Oceans. *J. Climate,* **11,** 1685–1702.
Slingo, J. M., D. P. Rowell, K. R. Sperber, and F. Nortley, 1999: On the predictability of the interannual behaviour of the Madden–Julian Oscillation and its relationship with El Niño. *Quart. J. Roy. Meteor. Soc.,* 583–609.
Stricherz, J., J. J. O'Brien, and D. M. Legler, 1992: *Atlas of Florida State University tropical Pacific winds for TOGA 1966–1985.* The Florida State University, 275 pp.
Thompson, C. J., 1998: Initial conditions for optimal growth in a coupled model of ENSO. *J. Atmos. Sci.,* **55,** 537–557.
Webster, P., 1994: The role of hydrological processes in ocean–atmosphere interactions. *Rev. Geophys.,* **32,** 427–476.
Weisberg, R. H., and T. Y. Tang, 1983: Equatorial ocean response to growing and moving wind systems with application to the Atlantic. *J. Mar. Res.,* **41,** 461–486.
Xue, Y., M. A. Cane, S. E. Zebiak, and T. N. Palmer, 1997: Predictability of a coupled model of ENSO using singular vector analysis. Part II: Optimal growth and forecast skill. *Mon. Wea. Rev.,* **125,** 2057–2073.
Zebiak, S., 1989: On the 30–60 day oscillation and the prediction of El Niño. *J. Climate,* **2,** 1381–1387.
——, and M. A. Cane, 1987: A model El Niño–Southern Oscillation. *Mon. Wea. Rev.,* **115,** 2262–2278.
Zhang, C., and H. H. Hendon, 1997: Propagating and standing components of the intraseasonal oscillation in tropical convection. *J. Atmos. Sci.,* **54,** 741–752.